Formation mechanism of defect metal hydrides containing superabundant vacancies

2007 J. Phys.: Condens. Matter 19 436201

(http://iopscience.iop.org/0953-8984/19/43/436201)

IOP PUBLISHING JOURNAL OF PHYSICS: CONDENSED MATTER

J. Phys.: Condens. Matter **19** (2007) 436201 (24pp) doi:10.1088/0953-8984/19/43/436201

Formation mechanism of defect metal hydrides containing superabundant vacancies

Yuh Fukai and Hidehiko Sugimoto[1]

Department of Physics, Chuo University, Kasuga, Bunkyo-ku, Tokyo 112-8551, Japan

E-mail: sugimoto@phys.chuo-u.ac.jp

Received 20 July 2007, in final form 3 September 2007
Published 26 September 2007
Online at stacks.iop.org/JPhysCM/19/436201

Abstract

The formation of defect hydrides containing a large number of M-atom vacancies (superabundant vacancies; SAVs) was studied in bcc NbH_x and in the fcc phase of FeH_x, CoH_x, NiH_x and PdH_x, by resistivity and XRD measurements under different conditions of hydrogen pressure and temperature, with/without allowing for exchange of hydrogen with environment (open-/closed-system methods). Two distinctly different behaviors were observed: in metals with small formation energy of Vac–H clusters, both H and vacancies enter abundantly into the M-lattice to form the ultimate defect-ordered structure, whereas in metals with relatively large formation energies, vacancy concentrations remain relatively small. This general trend was examined by Monte Carlo simulations based on a lattice–gas model. The result showed the occurrence of two distinct phases in the vacancy distribution caused by the combined action of the long-range elastic interaction and local Vac–H interactions, in accordance with the observation. Conditions for the occurrence of these 'vacancy-rich' and 'vacancy-poor' states are examined.

1. Introduction

In 1993, we discovered that gradual lattice contraction took place when Ni and Pd specimens were placed under high H_2 pressures and high temperatures, and concluded that it was due to the formation of a large number of M-atom vacancies amounting to ∼10 at.% [1, 2]. Since then, similar observations have been made in several other M–H alloys as well, and the formation of defect structures with superabundant vacancies (SAVs) is now recognized as one of the fundamental properties of M–H alloys [3–25].

Some other consequences of SAV formation have also been observed, of which the most important is the enhancement of M-atom diffusion. The enhancement in the presence of interstitial H, amounting to many orders of magnitude, was observed in the inter-diffusion in Pd–Ag [26], Cu–Ni [27] and Au–Fe [28–30] systems, and in the self-diffusion in Nb [18, 31, 32].

[1] Author to whom any correspondence should be addressed.

The mechanism of SAV formation is believed to be the trapping of H atoms by M-atom vacancies. In the presence of interstitial H atoms, the energy necessary to form a vacancy–H cluster ($VacH_r$) e_f^{cl} should become lower than the formation energy of a vacancy e_f^v approximately by a sum of binding energies e_{bi} [5],

$$e_f^{cl} \approx e_f^v - \sum_{i=1}^{r} e_{bi}. \tag{1}$$

The Vac–H interaction was studied extensively in 1980s in connection with plasma–wall interactions in fusion-reactor research, and binding energies were determined in a fairly large number of metals by e.g. implantation–annealing experiments [23–25, 32, 33]. The values thus obtained, ranging between $e_b = 0.1$ and 0.8 eV, are large enough to cause appreciable reduction of vacancy formation energies. The reduction effect can be more pronounced if, as suggested by theoretical calculations, a single vacancy can trap a multiple number of H atoms (i.e. the occupation number $r > 2$).

Regarding the configuration and energetics of Vac–H clusters, a general conclusion of theoretical calculations is that the binding energies are largest for single- and double-occupancies, becoming smaller for higher occupancies due to repulsion between trapped H atoms [34, 35]. In fcc and bcc metals, the maximum occupation number is usually assumed to be $r = 6$, where all the nearest octahedral (O) site of a vacancy are occupied by H atoms. A recent calculation for Al suggested, however, that the occupation number could be as large as $r = 12$ [36]. It should be noted that the binding energy is measured from the energy of a normal interstitial H atom, whereas the stability of a $VacH_r$ cluster in a given situation is determined by the energy of a trapped H atom relative to the chemical potential of H of the environment. For example, Tateyama and Ohno [35] showed that, in bcc Fe, $VacH_6$ can be stable in high pressure H_2 (∼GPa), whereas in vacuum only the Vac–H clusters of lower occupancy ($VacH_{2-3}$) are stable.

Experimentally, evidence of multiple occupancy has remained rather unclear. The configuration determined by ion channeling dealt exclusively with single-occupancy; a trapped H atom is displaced slightly (∼10%) from its original position toward a vacancy. No data are available for the configuration of multiple occupancies. Different binding energies manifested as multiple annealing (or desorption) stages in implantation–annealing (or thermal desorption) experiments have been assigned to successive detrapping from single vacancies, di-vacancies and vacancy aggregates (voids). In no case have separate detrapping stages of multiple H atoms from a single vacancy been identified [17, 25]. Note, however, that these observations do not contradict the occurrence of multiple occupancies, because Vac–H clusters of multiple occupancy, once formed under high H chemical potentials, should be subject to partial detrapping under ambient conditions, to be detected as clusters of lower occupancy in later analyses.

A possibility exists that a multiple trapping may be revealed by *in situ* measurements of the concentration of Vac–H clusters x_{cl} as a function of temperature and H concentration $x = [H]/[M]$, as the equilibrium condition for the chemical reaction $Vac + rH \rightleftarrows VacH_r$ leads to $x_{cl} \propto x^r \exp(-e_f^{cl}/kT)$; $e_f^{cl} \approx e_f^v - \sum_{i=1}^{r} e_{bi}$ for low concentrations of H and Vac–H clusters ($x, x_{cl} \ll 1$) [5, 9]. This dependence on the H concentration at a given temperature has not been verified by experiments so far. Instead, evidence of multiple trapping was obtained from the temperature dependence. The dependence of x_{cl} on temperature for a given H concentration is, in fact, more complicated because the occupation number is also an implicit function of temperature, tending from the fully occupied state at low temperatures to partially dissociated states at high temperatures. As the average occupation number r decreases with increasing temperature, the cluster formation energy e_f^{cl} increases, leading to concomitant decrease of

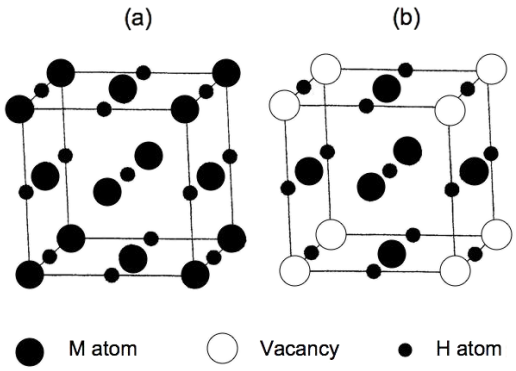

Figure 1. The crystal structure of fcc-based mono-hydride of NaCl-type (a), and vacancy-ordered M_3VacH_4 (b). In the vacancy-ordered structure, one of the four simple-cubic M-sublattices become vacant ($L1_2$ structure of Cu_3Au type), with octahedral interstitial sites filled with H atoms.

the concentration x_{cl}. This expected temperature dependence was observed in the Nb–H system [31].

There is another unique feature of defect-hydride formation which sometimes shows up at high concentrations of SAVs. In addition to uniform lattice contraction, in fcc M–H alloys, we observed superlattice XRD lines having simple-cubic indices, which we attributed to the formation of a vacancy-ordered $L1_2$ structure, M_3VacH_4 (a Cu_3Au-type M-lattice with O-sites filled with H atoms). This structure is shown in figure 1. Vacancies occupy one of the four simple-cubic sublattices of the fcc M-lattice, with each vacancy surrounded by 6 H atoms. This vacancy-ordered structure was observed in Ni–H [12], Pd–H [2, 10] and Mn–D [11] systems. Electronic calculations performed on this structure [10, 37–39] also showed that, in a series of 3d- and 4d-transition metals, the vacancy-ordered hydrides of this structure have lower energies than vacancy-free NaCl-type mono-hydrides [39]. In the Pd–H system under different conditions [8, 40], a different vacancy-ordered hydride of body-centered tetragonal structure was also observed, in which vacancies occupy 50% of one of the two M-sublattices randomly [40], and in the bcc phase of the Fe–H system, a vacancy-ordered CsCl-type structure was observed [41]. Note that the vacancy-ordered structure of bct Pd–H has close similarity to the vacancy-ordered CsCl structure of the Fe–H system; the only difference appears to be the occurrence of tetragonality in the former. As the composition of the former is Pd_3VacH_4, the composition of the latter may also be close Fe_3VacH_4.

Noteworthy is the fact that, in all these structures, vacancies order on 2nd-neighbor M-sites. This implies that the interaction between vacancies is repulsive on nearest-neighbor sites, and attractive on 2nd-neighbor sites. Thus, in forming the vacancy-ordered hydride structure, the vacancy–vacancy interaction of this nature should be operating, in addition to the attractive interaction between neighboring vacancy and H atom.

In the present paper, we re-examine the data accumulated in our laboratory in the last 15 years, and with a help of model calculations, try to clarify the formation process of SAVs, including the $x_{cl} - x$ relation, and the formation of the vacancy-ordered structure.

2. Experimental details

To investigate the formation of SAVs, two different methods have been adopted; the resistometry and the XRD. Owing to the high sensitivity of resistance measurements, the

Vac–H concentration may be determined to $x_{cl} \sim 10^{-3}$, provided the stability of measuring conditions is assured. The sensitivity of XRD measurements is admittedly lower, and allows the determination of x_{cl} to several at.%. In any case, *in situ* measurements are essential because SAVs may gradually disappear after recovery to ambient conditions.

Experiments are further divided into two groups; those performed by a closed-system method, and by an open-system method. The closed-system method was adopted for metals which form stable hydrides. Samples were prepared in advance, and the process of introduction as well as the ultimate equilibrium concentration of SAVs was determined under fixed H concentrations. The open-system method, on the other hand, was adopted in cases where the sample preparation (hydrogenation) could only be performed under high pHs, hence we were obliged to perform sample preparation and SAV formation measurement in a single experiment. The exchange of H between a sample and environment is allowed at a given pH, T condition, and hence the H concentration may vary in the course of SAV formation.

The resistometry was applied to Nb–H alloys (bcc structure) [18] in which, owing to large mobility of vacancies and high stability of hydrides, measurements could be performed by the closed-system method at medium temperatures ($\leqslant$300 °C) under ambient pressure within reasonable measuring times ($\leqslant$40 h).

Measurements on single-crystalline samples of Nb–H alloys showed that the resistance increase occurred in two stages; the first rapid process due to the introduction of SAVs from (or along) dislocations/grain boundaries, and the second slow process due to the introduction from external surface by bulk diffusion. In most cases, the former dominates over the latter; only in single crystals of high quality the latter becomes visible. From a series of such measurements, the equilibrium SAV concentration was found to be nearly proportional to H concentration ($x_{cl} \sim 1.3 \times 10^{-2} x$), in the range $x \leqslant 0.5$. (The absolute magnitude of x_{cl} could be off by a factor of 2 due to uncertainties in the value of resistivity increase caused by unit concentration of Vac–H clusters.)

By XRD, we measure lattice parameter changes to be caused by hydrogenation and SAV formation. These two processes occur in different time domains: the former can be completed typically within a few minutes whereas the latter takes much longer times of the order of hours. In most M–H alloys, to complete SAV formation within reasonable lengths of time, measurements should be performed at high temperatures ($\geqslant$800 °C), which in turn requires high H pressures ($p_H \geqslant 3$ GPa) to confine H in specimens. All the XRD measurements were performed by using synchrotron-radiation x-rays, the details of which were described elsewhere [11, 20].

In the case of PdH_x for $x < 0.8$, pre-fabricated samples of fixed H concentrations were sealed in high p_H, T conditions, and the lattice contraction due to introduction of Vac–H clusters was measured (a closed-system method) [20]. At high concentrations ($x \sim 1$), however, an open-system method had to be adopted, as described in the following [9]. Results of such measurements on PdH_x are shown in figure 2, together with those on NbH_x [42].

In other cases, FeH_x [19], CoH_x [21] and NiH_x [12], XRD measurements were made by the open-system method.

An example of XRD measurements is shown in figure 3 for γ-FeH_x [19]. Shortly after a pure Fe sample was heated to a prescribed temperature (1008 °C) under a high H pressure (pH = 5 GPa), the lattice parameter assumed a value ($a(0)$ at $t = 0$), larger than that of γ-Fe at a corresponding pH, T condition (a_0), and approached asymptotically a smaller value ($a(\infty)$) after sufficiently long times.

The H concentration at $t = 0$ can be estimated from the initial lattice expansion as

$$x(0) = \frac{\Omega(0) - \Omega_0}{\Omega_H}, \tag{2}$$

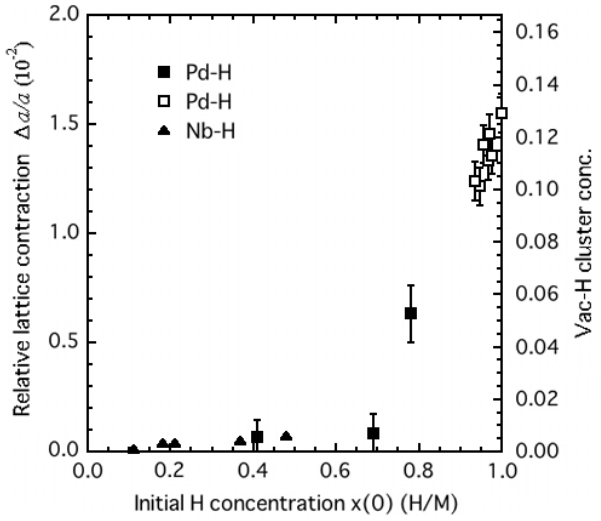

Figure 2. Relative lattice contraction of Pd, i.e. the fractional change of lattice parameters of the initial and final state, $\Delta a/a = (a(0)-a(\infty))/a(0)$, is plotted as a function of initial H concentration $x(0)$. Solid symbols from closed-system experiments [20] and open symbols from open-system experiments [9] (see the text). Concentrations of Vac–H clusters in Pd, approximately estimated by $(3\Delta a/a)/0.36$, can be read from the right scale. For Nb, the cluster concentration has been obtained from resistivity measurements by the closed-system method [18].

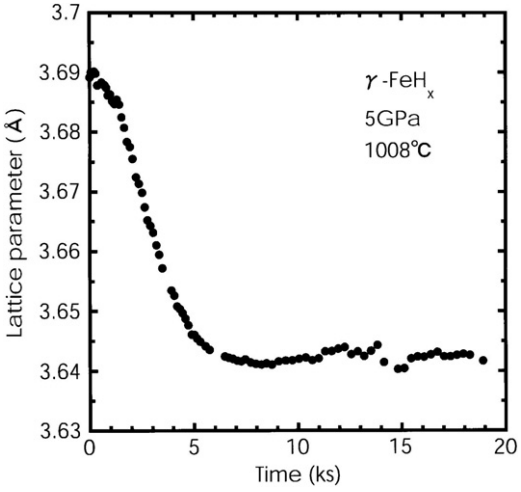

Figure 3. Lattice parameter as a function of time after hydrogenation, $a(t)$, of γ-FeH$_x$ (fcc) measured at pH = 5 GPa and $T = 1008\,^{\circ}$C [19]. From this graph, lattice parameters of the initial state $a(0)$ and the final state $a(\infty)$ are determined and compared with the lattice parameter of γ-Fe (fcc) at a corresponding p, T condition.

where $\Omega(0) = a(0)^3/4$ and $\Omega_0 = a_0^3/4$ for the fcc structure, and Ω_H is the H-induced volume expansion ($\Omega_H = 1.9\text{Å}^3$ for γ-FeH$_x$ [43][2]).

The implication of subsequent lattice contraction is more complex because the lattice contraction is a consequence of simultaneous changes of vacancy and H concentrations. Results

[2] A value obtained from the fcc alloy $Fe_{0.65}Mn_{0.29}Ni_{0.06}H_{0.95}$.

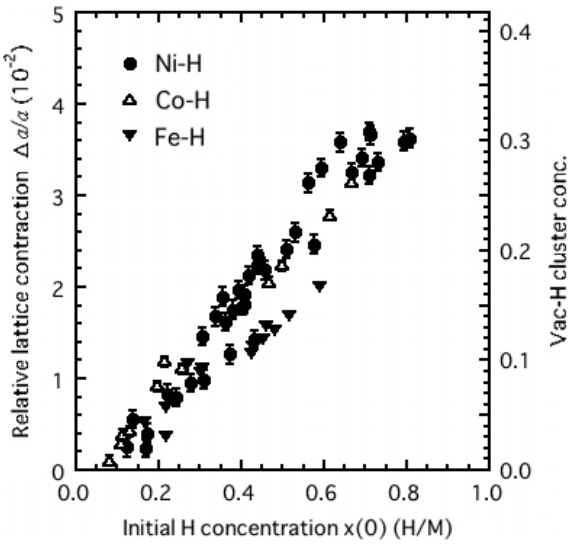

Figure 4. Relative lattice contraction, i.e. the fractional change of lattice parameters of the initial and final state, $\Delta a/a = (a(0) - a(\infty))/a(0)$, of samples of Fe, Co, and Ni in contact with H_2 at high pressures and temperatures (open-system experiments) is plotted as a function of initial H concentration $x(0)$. Concentrations of Vac–H clusters, approximately estimated by $(3\Delta a/a)/0.36$, can be read from the right scale [42].

of such measurements performed at different p_H, T conditions on the fcc phase of Fe–H, Co–H and Ni–H alloys are shown in figure 4 [19, 20, 42]. In this graph, the relative lattice contraction $\Delta a/a = (a(0) - a(\infty))/a(0)$ is plotted against the initial H concentration $x(0)$. On the right-hand axis is given an 'apparent' concentration of Vac–H clusters estimated from the relation

$$\tilde{x}_{cl} = \frac{\Omega(0) - \Omega(\infty)}{\Omega_{cl}}, \tag{3}$$

where $-\Omega_{cl}$ is the relaxation volume of a Vac–H cluster defined in terms of its formation volume as $v_f^{cl} = \Omega(0) - \Omega_{cl}$. Lacking experimental values of Ω_{cl}, we assumed $\Omega_{cl}/\Omega(0) \approx \Omega_v/\Omega_0 \approx 0.36$, the average of calculated values for vacancies (without trapped H atoms) in a number of fcc metals [44], and estimated the 'apparent' cluster concentration as $\tilde{x}_{cl} \approx (3\Delta a/a)/0.36$. In effect, this procedure ignores the possible lattice expansion to be caused by introduction of trapped H atoms, and therefore gives only a crude measure of the cluster concentration.

Figure 4 reveals an apparently simple relation that the lattice contraction is nearly proportional to the initial H concentration $x(0)$, irrespective of p_H, T conditions. This relation was quite unexpected, and appeared hardly acceptable at its face value. Thus, in an effort to identify the real implication of this relation, we re-plotted all the data of a_0, $a(0)$ and $a(\infty)$ measured at different pH, T conditions as a function of temperature T [42]. Results are shown in figures 5–7 for the fcc phase of Fe–H, Co–H and Ni–H systems. (Results for Pd–H alloys have been omitted because the data obtained by the open-system method are limited in number.)

These graphs reveal the following common features. The lattice parameter of a pure metal (a_0) shows a small increase with temperature as a result of thermal expansion. (The scatter is due to the effect of pressure, which is different for each data point.) What is significant here is that, although the lattice parameters immediately after hydrogenation ($a(0)$) assume

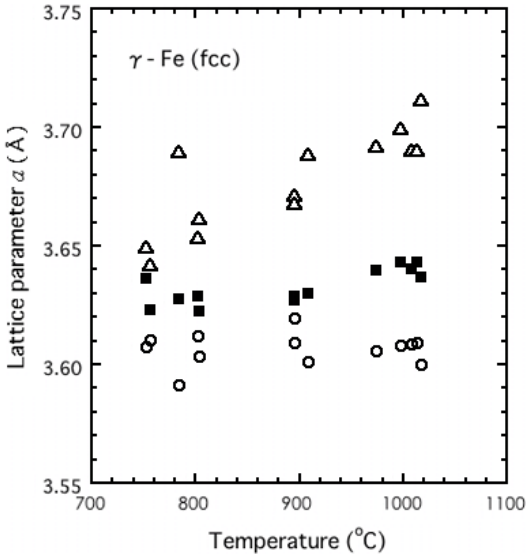

Figure 5. Comparison of the lattice parameters of γ-Fe (fcc) obtained under different p_{H}, T conditions. The lattice parameters of the initial state $a(0)$ (△), the final state after hydrogenation $a(\infty)$ (■), and that of the metal under the corresponding p, T condition a_0 (○), are plotted as a function of temperature.

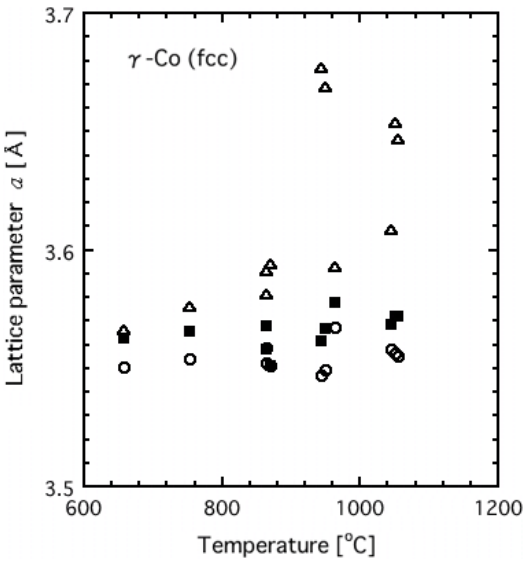

Figure 6. Comparison of the lattice parameters of γ-Co (fcc) obtained under different p_{H}, T conditions. The lattice parameters of the initial state $a(0)$ (△), the final state after hydrogenation $a(\infty)$ (■), and that of the metal under the corresponding p, T condition a_0 (○), are plotted as a function of temperature.

very different values depending on p_{H}, T conditions, the final lattice parameters ($a(\infty)$) resume nearly the same value slightly larger than a_0. In addition, $a(\infty)$ shows thermal

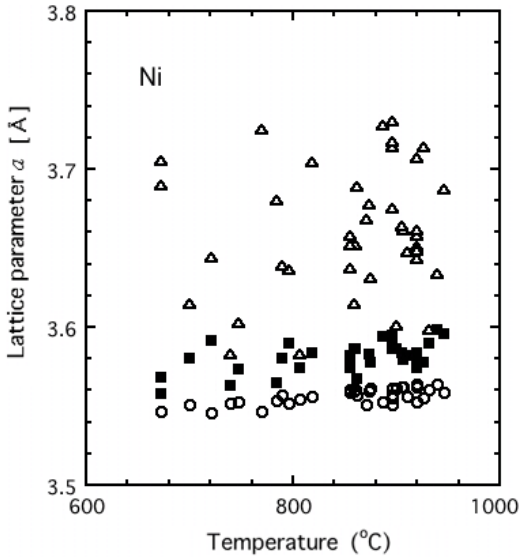

Figure 7. Comparison of the lattice parameters of Ni obtained under different p_H, T conditions [42]. The lattice parameters of the initial state $a(0)$ (○), the final state after hydrogenation $a(\infty)$ (■), and that of the metal under the corresponding p, T condition a_0 (○), are plotted as a function of temperature.

expansion similar to a_0. Thus, the apparent linear relation between the lattice contraction and initial H concentration was in fact a consequence of $a(\infty)$ being always close to a_0, namely, $\Omega(0) - \Omega(\infty) \approx 3a^2(a(0) - a(\infty)) \sim 3a^2(a(0) - a_0) \propto x(0)$.

These results indicate that, although the initial H concentrations are different for different pH, T conditions, samples in contact with surrounding H_2 finally attain the same ultimate structure having a fixed composition. In order to identify this ultimate structure, it is useful to recall the calculation of Zhang and Alavi [39]. They showed in their calculation for a series of 3d- and 4d-transition metals that lattice parameters of the vacancy-ordered hydride structure of composition M_3VacH_4 are much smaller than the corresponding vacancy-free hydrides and only slightly larger than those of original metals. Thus we presume that the ultimate structure attained after long holding times should be the defect structure having the composition M_3VacH_4. Although superlattice reflections to be caused by vacancy ordering were not observed in most of our experiments, probably due to high measuring temperatures, the final state is believed to have the composition close to this limit, with some short-range order remaining.

For the Pd–H system, shown in figure 2, the same argument can be made on the data obtained by the open-system method ($x(0) \sim 1$). For other data points ($x(0) < 0.8$) obtained by the closed-system method, no such complications exist, and the result can be taken at its face value. The Vac–H cluster concentrations remain small up to a critical concentration ($x \approx 0.7$) and increases thereafter. Results on Nb–H alloys follow the same trend at least up to $x \approx 0.5$.

Note that the process of formation of defect structures is distinctly different for two groups of metals, Fe, Co, Ni on one hand and Pd, Nb on the other. This difference in behavior may be correlated with the formation energy of a Vac–H cluster. Formation energies estimated from $e_f^{cl} \approx e_f^v - 6e_b$ using the known values of e_f^v and e_b are small ($e_f^{cl} = -0.01 - 0.08$ eV) for Fe, Co, Ni [20, 25], whereas those for Pd and Nb are much larger (0.72 eV for Pd [9] and 0.30 eV for Nb [18]).

Hence the following picture emerges for the formation of defect hydrides. In metals of small e_f^{cl}, both H and vacancies readily enter the metal lattice to attain the ultimate composition M_3VacH_4, whereas in metals of relatively large e_f^{cl}, cluster concentrations remain rather small up to some critical H concentration, approaching the ultimate composition thereafter.

This general trend will be examined by Monte Carlo simulations in the next section.

3. Theoretical

3.1. Formulation

Calculations are performed in the frame of a lattice–gas model, adopting a model Hamiltonian of the form

$$H = \tfrac{1}{2}\gamma B\Delta^2 V_0 + e_H n_H + e_v n_v + H_{int}, \tag{4}$$

where B is the bulk modulus, Δ is the lattice dilatation, γ is the image-force factor to include the free-surface effect [45, 46], e_H and e_v, and n_H and n_v, are the energy and number of H atoms and vacancies, respectively, in volume V_0, and H_{int} represents the interaction between H atoms and vacancies. The elastic interaction is included in the energy of an H atom and a vacancy, in the form,

$$e_H = u_H - \alpha_H\Delta, \tag{5a}$$

$$e_v = u_v + \alpha_v\Delta, \tag{5b}$$

where u_H is the energy of an isolated H atom, u_v is the formation energy of a vacancy ($= e_f^v$) in the absence of lattice dilatation, and α_H and α_v are taken to be positive. The implication of equation (5*a*) is that for introducing an interstitial H atom, which causes lattice expansion, the energy cost becomes smaller in an expanded lattice. The elastic interaction expressed in this way is known to provide a reasonable description of the spinodal decomposition in M–H systems; see, e.g. [47, 48]. For introducing a vacancy, which causes lattice contraction, the energy of formation becomes larger in an expanded lattice, as expressed by the positive sign in equation (5*b*).[3]

In the lattice–gas model adopted here, n_H is written as a sum of occupation numbers of H atoms on interstitial sites n_i^H, namely $n_H = \sum_i n_i^H$, where n_i^H assumes either 1 or 0 for occupied or unoccupied site i. Similarly, $n_v = \sum_l n_l^v$, with n_l^v either 1 or 0 for M-atom site l occupied or unoccupied by a vacancy, respectively. The interaction term is formally written as

$$H_{int} = \tfrac{1}{2}\sum_{i,j} J_{ij}^H n_i^H n_j^H + \tfrac{1}{2}\sum_{l,m} J_{lm}^v n_l^v n_m^v + \sum_{i,l} V_{il} n_i^H n_l^v, \tag{6}$$

with the three terms representing, in order, the H–H, Vac–Vac and H–Vac interactions, for which the following simplifying assumptions are made:

(1) No two H atoms can occupy the same interstitial site, and no direct interaction operates between any two H atoms.
(2) No two vacancies can occupy nearest M-atom sites.
(3) The interaction operates between a vacancy and an H atom on any nearest interstitial site. The interaction between the Vac–H pair is assumed to be attractive, with the interaction energy $V_{il} = -e_b$ ($e_b > 0$).

[3] The second term in equations (5*a*) and (5*b*) describing the elastic interaction should not be confused with a pv term in the enthalpy which should be added on to these equations, i.e. $h_H = e_H + p\Omega_H$ and $h_v = e_v + pv_f^v$. At high pressures, these pv terms are not really negligible, but their effect may be absorbed in the present formulation by simply increasing the values of u_H and u_v by appropriate amounts.

The partition function of the system is

$$Z = \int_{-\infty}^{\infty} \mathrm{d}\Delta \sum_{\{\mathrm{H}\}} \sum_{\{\mathrm{v}\}} \exp(-H/kT) = \sqrt{\frac{2\pi}{\gamma B V_0}} Z_1, \tag{7}$$

$$Z_1 = \sum_{\{\mathrm{H}\}} \sum_{\{\mathrm{v}\}} \exp(-H_1/kT), \tag{8}$$

where

$$H_1 = u_{\mathrm{H}} n_{\mathrm{H}} + u_{\mathrm{v}} n_{\mathrm{v}} - \frac{\alpha_{\mathrm{H}}^2}{2\gamma B V_0} \left(n_{\mathrm{H}} - \frac{\alpha_{\mathrm{v}}}{\alpha_{\mathrm{H}}} n_{\mathrm{v}} \right)^2 + H_{\mathrm{int}}. \tag{9}$$

Using this, thermal average quantities can be calculated;

$$\langle n_{\mathrm{H}} \rangle = \frac{1}{Z_1} \sum_{\{\mathrm{H}\}} \sum_{\{\mathrm{v}\}} n_{\mathrm{H}} \exp\left(-H_1/kT\right), \tag{10}$$

$$\langle n_{\mathrm{v}} \rangle = \frac{1}{Z_1} \sum_{\{\mathrm{H}\}} \sum_{\{\mathrm{v}\}} n_{\mathrm{v}} \exp(-H_1/kT), \tag{11}$$

and

$$\langle \Delta \rangle = (\alpha_{\mathrm{H}} \langle n_{\mathrm{H}} \rangle - \alpha_{\mathrm{v}} \langle n_{\mathrm{v}} \rangle)/\gamma B V_0. \tag{12}$$

In the absence of vacancies, we have $\alpha_{\mathrm{H}} = \gamma B \langle \Delta \rangle V_0 / \langle n_{\mathrm{H}} \rangle = \gamma B \Omega_{\mathrm{H}}$, and similarly $\alpha_{\mathrm{v}} = \gamma B \Omega_{\mathrm{cl}}$.

Actual calculations were performed for the fcc metal lattice consisting of $N_0 = 4000$ sites and an equal number of octahedral interstitial sites for H atoms, repeated by periodic boundary conditions. The parameters adopted are appropriate for Ni; $u_{\mathrm{v}} = 1.8$ eV [49], $\gamma = 0.4$ [46], $B = 190$ GPa, $\Omega_0 = 10.9$ Å^3 and $\Omega_{\mathrm{H}} = 2.2$ Å^3 [50], which gives $\alpha_{\mathrm{H}} = 1.04$ eV and $\alpha_{\mathrm{H}}^2/\gamma B \Omega_0 = \gamma B \Omega_{\mathrm{H}}^2/\Omega_0 = 0.2$ eV. For the parameter $\alpha_{\mathrm{v}}/\alpha_{\mathrm{H}}$, we assume a value 3.0, which is larger than expected for a vacancy without trapped H atoms, $\alpha_{\mathrm{v}}/\alpha_{\mathrm{H}} = \Omega_{\mathrm{v}}/\Omega_{\mathrm{H}} = 0.36 \times 10.9/2.2 = 1.8$. The reason for this choice will be described later.

Hereafter, the concentrations of H and vacancies are expressed as per site, i.e. $x = \langle n_{\mathrm{H}} \rangle / N_0$ and $x_{\mathrm{v}} = \langle n_{\mathrm{v}} \rangle / N_0$. They correspond, respectively, to x and x_{cl} used in the preceding section.

3.2. Calculation for the closed system

Monte Carlo calculations for the closed system were performed by Metropolis importance sampling method, allowing for introduction/removal of vacancies in a metal lattice containing a fixed number of H atoms.

In order to facilitate comparison with the experimental results shown in figure 2, the final concentration of vacancies $x_{\mathrm{v}}(\infty)$ was calculated as a function of H concentration x. The calculation was performed for several different temperatures, and five different values of the binding energy e_{b}. The results obtained for $kT = 0.10$ eV ($T = 1160$ K) and 0.15 eV (1740 K) are shown in figures 8(a) and (b), respectively. On the right-hand axis is given the volume contraction $\Omega(0) - \Omega(\infty) = \Omega_{\mathrm{cl}} x_{\mathrm{v}}(\infty)$ with $\Omega_{\mathrm{cl}} = 6.6$ Å^3.

For a given set of T, e_{b}, the actual calculation was performed by the following procedure:

(1) Start with a vacancy-ordered hydride M_3VacH_4, with $x_{\mathrm{v}}(0) = 0.25$ and $x = 1$.
(2) Decrease x by 0.05.
(3) Allow jumps of H atoms and introductions/removals of vacancies repeatedly until equilibrium is attained. Calculate the concentrations of vacancies by taking the average over 2400 000 subsequent repetitions (300 repetitions per site) in this equilibrium state.

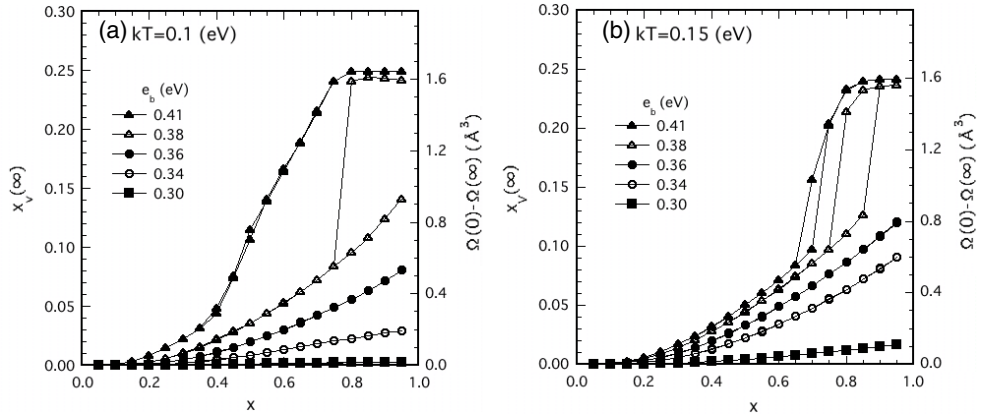

Figure 8. The vacancy concentration $x_v(\infty)$ calculated by Monte Carlo simulations as a function of H concentration x. The concomitant volume contraction $\Omega(0) - \Omega(\infty) = \Omega_{cl} x_v(\infty)$ is given on the right-hand axis. No exchange of H with environment is allowed (the closed-system method). Calculations have been performed at two temperatures, (a) $kT = 0.1$ eV (1160 K) and (b) 0.15 eV (1740 K), for five different values of the Vac–H binding energy e_b.

(4) Repeat (2) and (3) until x reaches 0.05.
(5) Increase x by 0.05 and repeat (3).
(6) Repeat (5) until x reaches 0.95.

Figures 8(a) and (b) show that an abrupt increase of x_v occurs at a certain value of e_b. This trend, indicating the occurrence of 'vacancy-rich' and 'vacancy-poor' phases, is more conspicuous at lower temperatures. At 1160 K, for $e_b > 0.41$ eV, x_v starts increasing from small values of x, and reaches a saturation at $x = 0.75 \sim 0.8$, whereas for $e_b < 0.36$ eV, it stays rather small over a wide range of x. In between, discontinuous changes of x_v occur at certain values of x, accompanied with a hysteresis. The vacancy concentration x_v in the 'vacancy-poor' phase increases at higher temperatures. Origin of these dependences on T, e_b and x will be examined in the next section.

Note that the volume contraction $\Omega(0) - \Omega(\infty)$ is related to the fractional lattice contraction $\Delta a/a$ defined in section 2 by

$$\Omega(0) - \Omega(\infty) \approx 3\Omega(0)\frac{\Delta a}{a}. \tag{13}$$

3.3. Calculation for the open system

Calculations for the open system were made in a similar way except that the introduction/removal of H atoms, as well as vacancies, is allowed. In this case, the initial H concentration $x(0)$ is adjusted by varying u_H, starting from a sufficiently low value of u_H and increasing it by steps.

The lattice contraction caused by the introduction of vacancies and H atoms was calculated as

$$\Omega(0) - \Omega(\infty) = \Omega_{cl} x_v(\infty) - \Omega_H(x(\infty) - x(0)). \tag{14}$$

The results are shown in figure 9, as a function of initial H concentration $x(0)$. The calculation was performed at a fixed temperature $kT = 0.1$ eV ($T = 1160$ K), for five different values of the binding energy e_b.

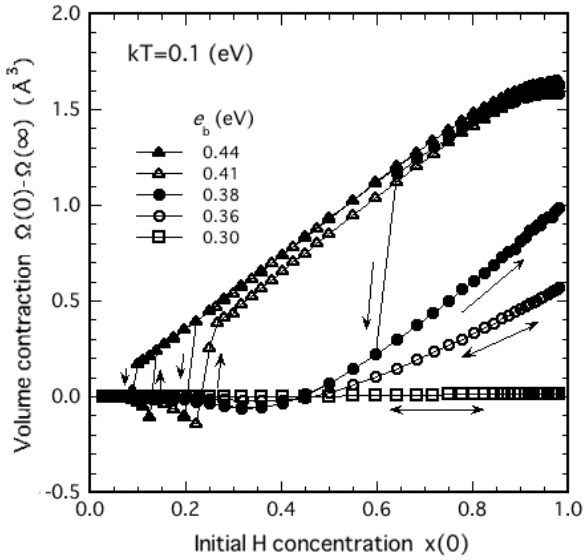

Figure 9. The volume contraction $\Omega(0) - \Omega(\infty)$ calculated by Monte Carlo simulations as a function of initial H concentration x (0). Exchange of H with environment is allowed (the open-system method). Calculations have been performed at $kT = 0.1$ eV (1160 K), for five different values of the Vac–H binding energy e_b. Note the appearance of hysteresis for intermediate values of e_b.

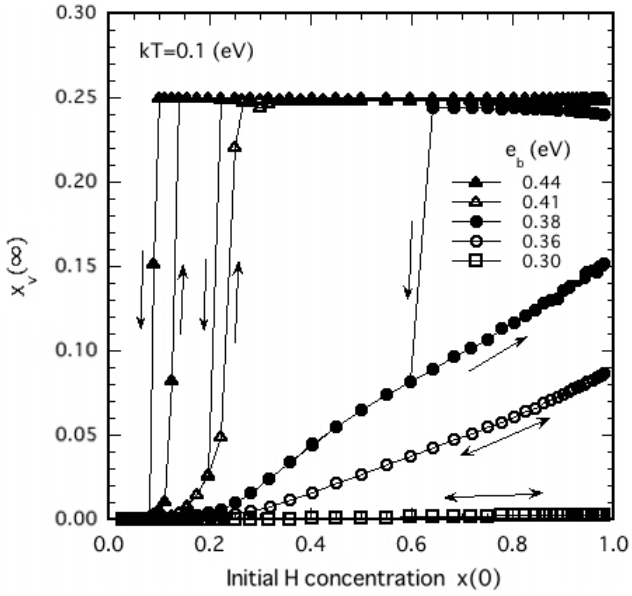

Figure 10. Final concentration of vacancies in the open system $x_v(\infty)$ as a function of initial H concentration $x(0)$, that underlie the volume contraction shown in figure 9. Calculations have been performed at $kT = 0.1$ eV (1160 K), for five different values of the Vac–H binding energy e_b. Note the strong tendency for the formation of M_3VacH_4 for large values of e_b.

The concentrations of vacancies and H atoms in the final state, $x_v(\infty)$ and $x(\infty)$, that have caused this volume change, are shown in figures 10 and 11, respectively, as a function of $x(0)$.

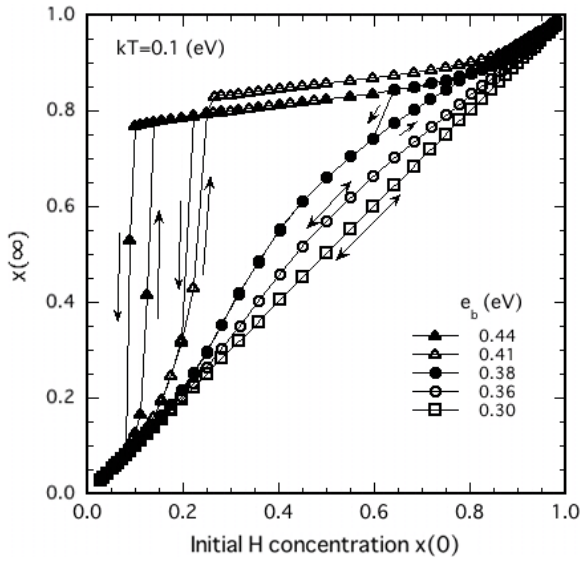

Figure 11. Final concentrations of H atoms in the open system $x(\infty)$ as a function of initial H concentration $x(0)$, that underlie the volume contraction shown in figure 9. Calculations have been performed at $kT = 0.1$ eV (1160 K), for five different values of the Vac–H binding energy e_b. Note the strong tendency for the formation of M_3VacH_4 for large values of e_b.

For strong binding ($e_b > 0.40$ eV), the composition quickly changes to $M_3VacH_{\sim 3}$ ($x_v(\infty) = 0.25$ and $x(\infty) \sim 0.8$) for any initial H concentrations. For weaker binding ($e_b < 0.36$ eV), on the other hand, smaller amounts of vacancies and H atoms are introduced. Note the appearance of hysteresis for the intermediate values of e_b.

Implication of these results will be examined in the next section.

4. Discussion

A key for understanding the anomalous SAV formation behavior in metal hydrides is the occurrence of two-phase separation in the vacancy distribution, caused by the combined action of long-range elastic interaction and local Vac–H interactions. Here we examine the implication of these interactions, and proceed to interpret the experimental results in light of this.

4.1. Implication of long-range elastic interaction

The free energy, calculated by taking the thermal average of equation (9), reads

$$F = \langle H \rangle - T \langle S_c \rangle = u_H \langle n_H \rangle + u_v \langle n_v \rangle - \frac{1}{2\gamma B V_0} [\alpha_H \langle n_H \rangle - \alpha_v \langle n_v \rangle]^2 + \langle H_{int} \rangle - T \langle S_c \rangle , \tag{15}$$

where a term $kT/2$ arising from the averaging of Δ^2 has been neglected.

In the familiar case of M–H systems, where the formation of M-atom vacancies is disregarded, the chemical potential of hydrogen is obtained from this expression by placing $\langle n_v \rangle = 0$ and differentiating, namely,

$$\mu_H = \frac{\partial F}{\partial \langle n_H \rangle} = u_H - \frac{\alpha_H^2}{\gamma B \Omega_0} x + \frac{1}{N_0} \frac{\partial \langle H_{int} \rangle}{\partial x} - \frac{T}{N_0} \frac{\partial \langle S_c \rangle}{\partial x}. \tag{16}$$

If the interaction term is neglected, this reduces to the ordinary form

$$\mu_{\mathrm{H}} = u_{\mathrm{H}} - \overline{u_{\mathrm{H}}}x + kT \ln \frac{x}{x_0 - x}, \tag{17}$$

where $\overline{u_{\mathrm{H}}} = \alpha_{\mathrm{H}}^2/\gamma B\Omega_0$ and x_0 is the maximum H concentration. As is well known, the presence of the second term, representing the long-range elastic interaction, leads to two-phase separation (called the spinodal decomposition) of H distribution, with a critical point located at [48]

$$x_{\mathrm{c}} = x_0/2 \qquad \text{and} \qquad 4kT_{\mathrm{c}} = x_0\overline{u_{\mathrm{H}}}. \tag{18}$$

In the present calculation, the parameters adopted for Ni ($x_0 = 1$ and $\overline{u_{\mathrm{H}}} = 0.2$ eV) leads to $T_{\mathrm{c}} = 580$ K, which agrees excellently with the observation [51, 52].

For vacancies, the chemical potential can be calculated similarly;

$$\mu_{\mathrm{v}} = \frac{\partial F}{\partial \langle n_{\mathrm{v}} \rangle} = u_{\mathrm{v}} - \frac{\alpha_{\mathrm{v}}^2}{\gamma B\Omega_0}\left(x_{\mathrm{v}} - \frac{\alpha_{\mathrm{H}}}{\alpha_{\mathrm{v}}}x\right) + \frac{1}{N_0}\frac{\partial \langle H_{\mathrm{int}} \rangle}{\partial x_{\mathrm{v}}} - \frac{T}{N_0}\frac{\partial \langle S_{\mathrm{c}} \rangle}{\partial x_{\mathrm{v}}}. \tag{19}$$

Thus we expect that a linear dependence of μ_{v} on x_{v} should lead to similar spinodal decomposition in the vacancy distribution, with a critical point located at

$$x_{\mathrm{vc}} = x_{\mathrm{v}0}/2 \qquad \text{and} \qquad 4kT_{\mathrm{vc}} = x_{\mathrm{v}0}\overline{u_{\mathrm{v}}}. \tag{20}$$

Substituting $x_{\mathrm{v}0} = 1/4$ and $\overline{u_{\mathrm{v}}} = \alpha_{\mathrm{v}}^2/\gamma B\Omega_0 = 9\overline{u_{\mathrm{H}}}$, we obtain $T_{\mathrm{vc}} = 9/4T_{\mathrm{c}} = 1305$ K.

These calculations suggest that the abrupt change of the $x_{\mathrm{v}}(\infty)$–x relations, shown in figures 8(a) and (b), may be a consequence of the two-phase separation in the vacancy distribution to be caused by the long-range elastic interaction. When examined more closely, however, we note that this could not be the sole origin of the two-phase separation. The phase separation still existing at 1740 K, much higher than the critical temperature calculated for the spinodal decomposition (1305 K), indicates that some additional mechanism must be operating to incite the phase separation. That this is due to the Vac–H interaction in equation (19), disregarded in the above discussion, will be shown in section 4.2.

Here we add some descriptions regarding the strength of the elastic interaction. The reason for choosing the parameter, $\alpha_{\mathrm{v}}/\alpha_{\mathrm{H}} = 3$ ($\Omega_{\mathrm{cl}} = 6.6$ Å^3), has been to bring the lattice parameter of M_3VacH_4 into agreement with experiments. In comparison to $\alpha_{\mathrm{v}}/\alpha_{\mathrm{H}} = \Omega_{\mathrm{v}}/\Omega_{\mathrm{H}} = 1.8$ ($\Omega_{\mathrm{v}} = 4.0$ Å^3), legitimate for an isolated vacancy, this assumes in effect that the lattice contraction around a vacancy with trapped H atoms should be larger than that of an isolated vacancy. This may be more easily understandable as a convention to describe smaller lattice expansion around an H atom trapped by a vacancy. Evidence in support of this has been provided by our high p, T experiments, which showed that the reduction of the equilibrium cluster concentration due to a $pv_{\mathrm{f}}^{\mathrm{cl}}$ term in the formation enthalpy is small even at pressures of several GPa. Under those conditions, isolated vacancies in metals having the formation volume of $v_{\mathrm{f}}^{\mathrm{v}} \sim (1-0.36)\Omega_0 = 7$–$10$ Å^3, hence $pv_{\mathrm{f}}^{\mathrm{v}} = 0.2$–$0.3$ eV for $p = 5$ GPa, should be subject to appreciable reductions of the equilibrium concentration. The reason why the formation volume of a Vac–H cluster $v_{\mathrm{f}}^{\mathrm{cl}} = \Omega_0 - \Omega_{\mathrm{cl}}$ becomes much smaller is because the relaxation volume—Ω_{cl} is larger in magnitude to compensate for a greater part of Ω_0. The smallness of the $pv_{\mathrm{f}}^{\mathrm{cl}}$ term justifies the comparison of the present calculation with experiments performed at high pressures.

4.2. Analysis of the results for the closed system

To help identifying the effect of local Vac–H interaction, we performed another calculation in which the elastic interaction due to vacancies is assumed non-existent ($\alpha_{\mathrm{v}} = 0$ in equation (5*b*)).

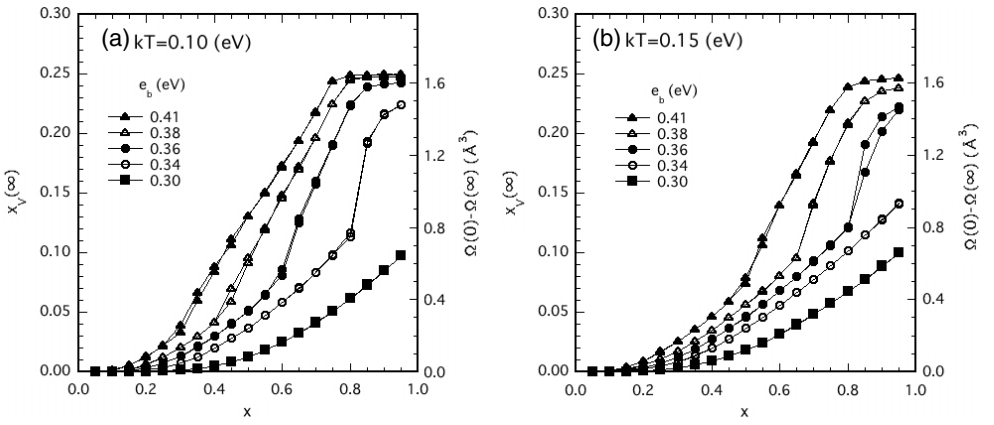

Figure 12. The $x_v(\infty)$ versus x relation calculated for the closed system at two temperatures, (a) $kT = 0.1$ eV (1160 K) and (b) 0.15 eV (1740 K), without including the effect of elastic interaction on vacancies ($\alpha_v = 0$). The concomitant volume contraction $\Omega(0) - \Omega(\infty) = \Omega_{cl} x_v(\infty)$ is given on the right-hand axis. Comparison with the corresponding results for $\alpha_v = 3\alpha_H$ (figure 8) reveals the disappearance of hysteresis in the phase transitions.

The results are shown in figures 12 (a) and (b), for temperatures $kT = 0.1$ eV (1160 K) and 0.15 eV (1740 K), respectively. Two-phase separation does indeed take place in these cases as well. The transition from the 'vacancy-poor' state to the 'vacancy-rich' state occurs more easily at a lower temperature: it starts from lower H concentrations, and smaller values of e_b. A more important feature becomes manifest when these results are compared with the corresponding results of finite elastic interactions (figures 8(a) and (b)). The results are closely similar for large values of e_b!

We conclude from these results that the effect of local configuration of vacancies and H atoms is playing an equally important role in the two-phase separation process. Configurations accommodating larger numbers of Vac–H bonds have lower internal energies, and are therefore more preferable energetically. Thus, for a given number of vacancies and H atoms, the lowest-energy configuration should be the one in which the total number of Vac–H bonds is maximum. Note, in particular, that in the vacancy-ordered structure M_3VacH_4 a large fraction of H atoms create two Vac–H bonds per H atom, in this way leading to the maximum lowering of the internal energy. Thus, the Vac–H interaction should lead to the formation of the 'vacancy-rich' phase precipitating out of a 'vacancy-poor' phase, coexisting with the latter. This tendency will become stronger for larger values of e_b. At finite temperatures, however, as the clustering of vacancies is accompanied by the loss of configurational entropy, the 'vacancy-rich' state should become less stable, and transform to the 'vacancy-poor' state having a larger configurational entropy. Local configurational effects such as this have been ignored in the average elastic interaction, but have been included automatically in the Monte Carlo simulation. The fact that for large e_b the calculations for $\alpha_v/\alpha_H = 0$ and 3 agree closely with each other indicates that the local Vac–H interaction is dominant in these cases.

The reason why for large e_bs the ultimate vacancy concentration $x_v(\infty) = 0.25$ is attained above $x = 0.75$ can be understood by inspection of the crystal structure. Figure 1 shows, in M_3VacH_4, 3/4 of H atoms have two neighboring vacancies, whereas the remaining 1/4 H atoms have no neighboring vacancies. This implies that $x = 0.75$ is large enough to provide six H atoms to each vacancy, to induce maximum reduction of the total energy.

Another feature of the 'vacancy-poor' state becomes apparent when $x_v(\infty)$ versus x relations at different temperatures are compared. In figure 13 are shown such relations at three

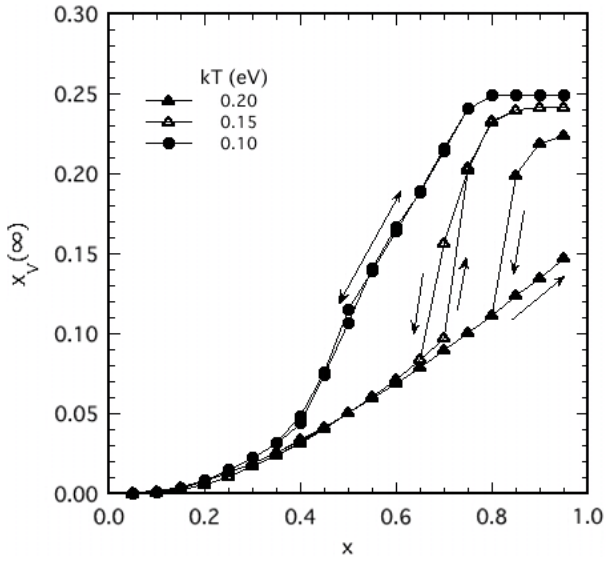

Figure 13. The $x_v(\infty)$ versus x relation calculated for the closed system for three different temperatures $kT = 0.10$, 0.15 and 0.20 eV (1160, 1740 and 2320 K). $e_b = 0.41$ eV and $\alpha_v = 3\alpha_H$.

different temperatures, for a particular value of the binding energy, $e_b = 0.41$ eV. A notable feature is that the $x_v(\infty)$ versus x relation of the 'vacancy-poor' state converges to a common curve, giving endorsement to the existence of a well-defined defect state. The fact that this 'vacancy-poor' state is realized over wide H concentrations at high temperatures, and that the common curve approaches $\sim 1/2$ of the maximum vacancy concentration ($x_v(\infty) = 0.25$) at $x = 1.0$, suggest that this must be the state of maximum configurational entropy.

Figure 14 shows the temperature dependence of $x_v(\infty)$ for two representative values of the binding energy, $e_b = 0.41$ and 0.34 eV, at two different H concentrations, $x = 0.50$ and 0.95. For a large binding energy $e_b = 0.41$ eV, the transition between the 'vacancy-rich' and 'vacancy-poor' states takes place, whereas no such transition takes place for a small binding energy $e_b = 0.34$ eV. There, the system stays in the 'vacancy-poor' state at all temperatures, with $x_v(\infty)$ increasing monotonously with increasing temperature.

The constitution of the 'vacancy-rich' and 'vacancy-poor' states can be made more manifest by the population analysis, namely, by counting the number of Vac–H bonds in the course of phase transition. The average local configuration around an H atom can be examined by counting the number of isolated H atoms, H–Vac and H–Vac_2 complexes.

Results of such population analysis are shown in figures 15 and 16 for $e_b = 0.41$ and 0.34 eV, respectively. The H concentration is fixed at $x = 0.95$, where most of the interstitial sites are filled.

For a large binding energy $e_b = 0.41$ eV, figure 15 shows that at low temperatures the fraction of H atoms with two neighboring vacancies is $\sim$0.80, those with one vacancy is $\sim$0, and those without vacancies is $\sim$0.10, consistent with the ordered structure shown in figure 1. Above the phase transition temperature $kT \sim 0.20$ eV ($\sim$2300 K), the fractions change to $\sim$0.10, 0.60 and 0.30, respectively, showing the formation of predominantly H–Vac pairs. Thus, the high-temperature phase is a disordered state having a larger configurational entropy. (The reason why the populations do not return to the original values upon cooling is probably due to the finite size and timescale of the simulation.) The average binding energy per H atom

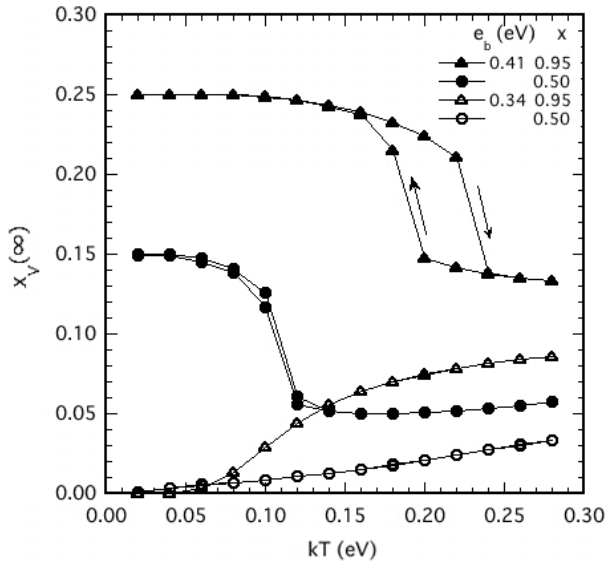

Figure 14. Temperature dependence of the vacancy concentration calculated for the closed system, for $e_b = 0.34$ and 0.41 eV, and $x = 0.50$ and 0.95.

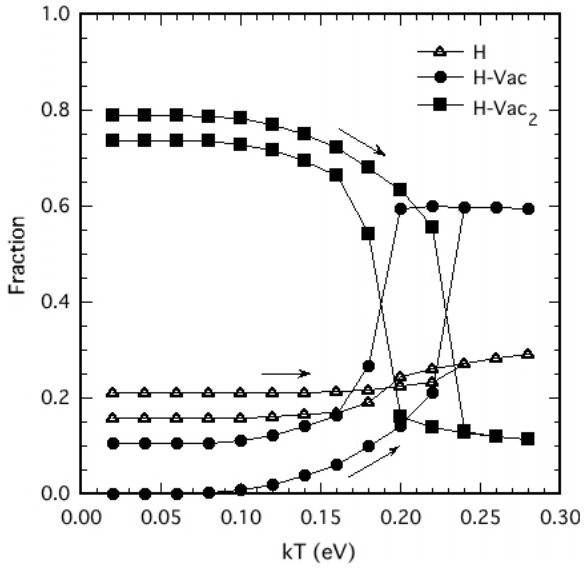

Figure 15. Temperature dependence of the fraction of H atoms of three different configurations (H, H–Vac and H-Vac_2), calculated for the closed system with $e_b = 0.41$ eV and $x = 0.95$. Note the abrupt population changes across the phase transition at $kT \approx 0.2$ eV.

can also be estimated; $0.8 \times 2e_b$ for the low-temperature state, and $(0.1 \times 2 + 0.6 \times 1)e_b$ for the high-temperature state. The average binding energy thus decreases to $\sim 1/2$ in the high-temperature state. In brief, the nature of the phase transition is the first-order transition in the vacancy sublattice, in which the total number as well as the distribution of vacancies is changed.

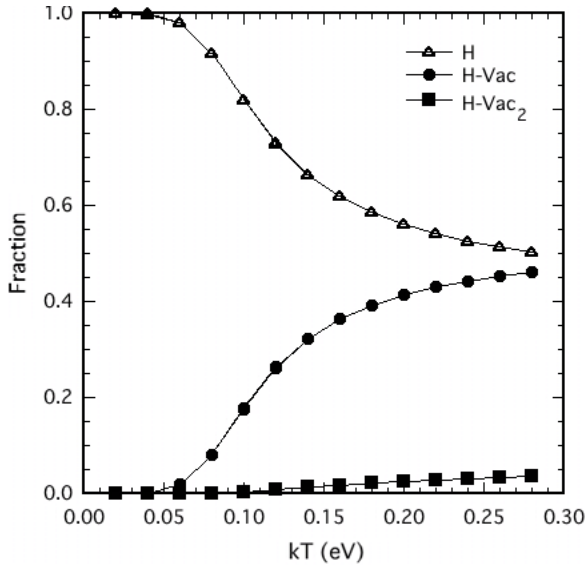

Figure 16. Temperature dependence of the fraction of H atoms of three different configurations (H, H–Vac and H-Vac_2), calculated for the closed system with $e_b = 0.34$ eV and $x = 0.95$. Note the gradual population changes in the 'vacancy-poor' phase.

Figure 16 shows that the case of low binding energy, $e_b = 0.34$ eV, is very different. At low temperatures, no H atoms are associated with vacancies, simply because vacancies do not exist. As temperature is raised, an increasing number of H atoms become associated with vacancies, mostly in the form of H–Vac pairs. The fraction of H–Vac_2 complexes remains small. Note that, at high temperatures, the fraction of H–Vac pairs is close to six times the vacancy concentration shown in figure 14. In this case, where the system remains in the 'vacancy-poor' state at all temperatures, the formation of vacancies is driven by the configurational entropy of vacancies in the M-sublattice.

Additional information can be obtained from another type of population analysis, i.e. from the local configuration around a vacancy, by counting the number of $VacH_6$, $VacH_5$, $VacH_4$ ... clusters. At high H concentrations ($x = 0.95$), such population analysis showed that the fraction of $VacH_6$ is always close to 1, as it should, with a slight signature of partial dissociation above $kT \geqslant e_b/4$.

The population analysis for the intermediate H concentration $x = 0.50$ is shown in figure 17 for $e_b = 0.41$ eV. Below the transition temperature ($kT \sim 0.11$ eV), the local configuration around H atoms is similar to figure 15. The fact that nearly 85% of H atoms are in the form of H–Vac_2 implies that most of H atoms (and vacancies) are contained in the 'vacancy-rich' phase, leaving the 'vacancy-poor' phase almost depleted of H atoms (and vacancies). The system is divided into nearly equal amounts of 'vacancy-rich' and 'vacancy-poor' phases. A notable difference from figure 15, i.e. the absence of isolated H atoms in the lower-temperature phase, indicates that the 'vacancy-rich' phase has a composition M_3VacH_3, where H atoms do not occupy one of the four sublattices of O-sites (the body-centered site in figure 1).

Local configuration around vacancies, obtained for the intermediate H concentration ($x = 0.50$), is shown in figure 18. In the lower-temperature region ($kT < 0.11$ eV), the fraction of $VacH_6$ is 100%, consistent with the vacancy-ordered structure M_3VacH_3, whereas at $kT > 0.11$ eV, an increasing number of Vac–H clusters dissociate with increasing temperature.

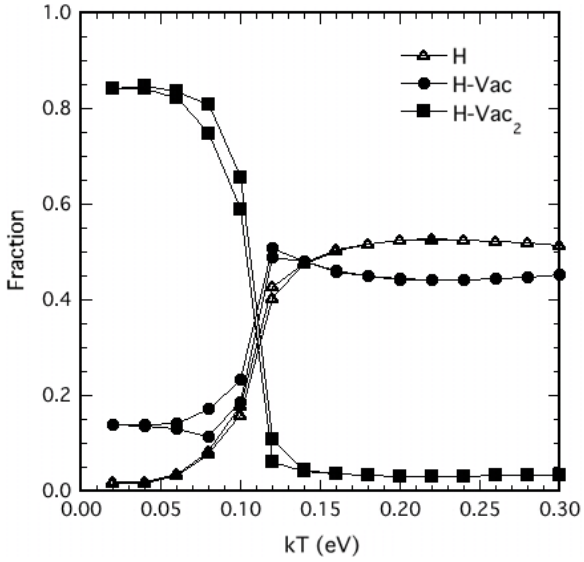

Figure 17. Temperature dependence of the fraction of H atoms of three different configurations (H, H–Vac and H–Vac_2), calculated for the closed system with $e_b = 0.41$ eV and $x = 0.50$.

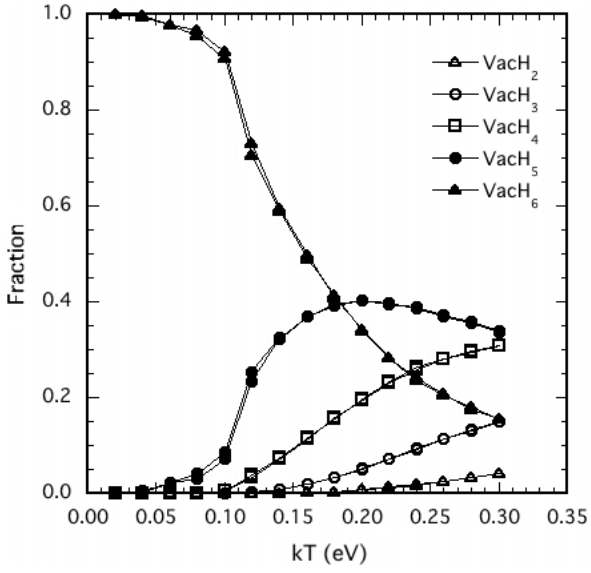

Figure 18. Temperature dependence of the fraction of vacancies of different configurations ($VacH_n$; $n = 1$–6), calculated for the closed system with $e_b = 0.41$ eV and $x = 0.50$.

Figure 19 shows the temperature dependence of the vacancy concentration for $e_b = 0.41$ eV, calculated for several different H concentrations. The case of highest H concentration ($x = 0.95$) corresponds to the transition from the perfectly vacancy-ordered state to the vacancy-disordered state, as described above. As H concentration is lowered, both the transition temperature and the vacancy concentration in the lower-temperature region become lower. The decrease of vacancy concentration in the lower-temperature region is a consequence of the

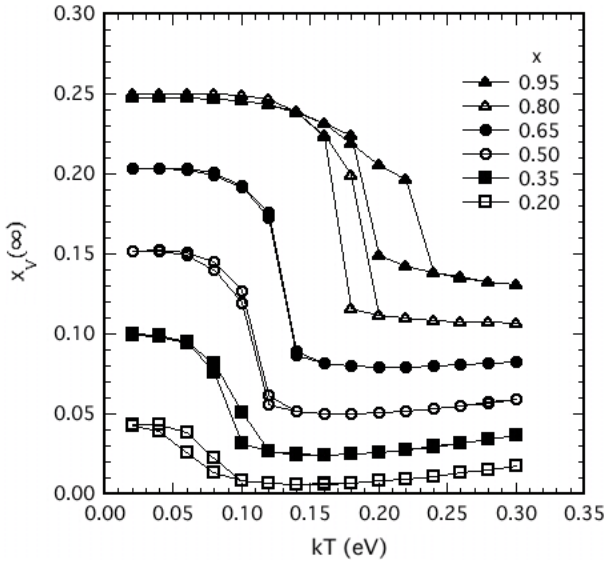

Figure 19. Temperature dependence of the vacancy concentration for several different H concentrations, calculated for the closed system with $e_b = 0.41$ eV.

decreasing amount of the 'vacancy-rich' phase. The decrease of the transition temperature with decreasing H concentrations, on the other hand, should be due to the increase of the configurational entropy of the 'vacancy-poor' phase.

Generally speaking, the constitution of defect hydrides is a very complex problem, especially at intermediate H concentrations, because the configurational entropy as well as the internal energy of the system depends in a complex way on the concentration of H atoms and vacancies interacting with each other. The fact that the total number of vacancies is not conserved adds to the complexities. To avoid intricate descriptions of the problem, here we focus on the following two specific aspects.

Let us start by examining the contribution of the interaction terms to the chemical potential of vacancies. Substituting numbers appropriate for Ni into equation (19), we obtain

$$\mu_v[\mathrm{eV}] = 1.8 - 1.8x_v + 0.6x + \frac{1}{N_0}\frac{\partial\langle H_{\mathrm{int}}\rangle}{\partial x_v} - \frac{T}{N_0}\frac{\partial\langle S_c\rangle}{\partial x_v}. \tag{21}$$

Note that the effect of elastic interaction ($0.6x$ eV) is rather large and tends to suppress the SAV formation at high H concentrations. The local interaction term can be written approximately as a thermal average of the binding energy per vacancy, $N_0^{-1}\partial\langle H_{\mathrm{int}}\rangle/\partial x_v \approx -\langle\sum_i e_{bi}\rangle$. This term, being always close to $-6e_b$, depends only weakly on H concentration, and decreases slightly in magnitude with increasing temperature. Thus, for smaller e_bs, the elastic interaction dominates to keep the system in the 'vacancy-poor' state, whereas for large e_bs, the local interaction dominates to create the 'vacancy-rich' state.

A more quantitative analysis of vacancy formation, including its dependence on temperature and H concentration, can be made in the 'vacancy-poor' state. Figure 20 shows the Arrhenius plot of the vacancy concentration for $e_b = 0.34$ eV, for three different H concentrations. The Arrhenius plot forms straight lines at low vacancy concentrations, $x_v \leqslant 0.03$, showing that the vacancy (Vac–H cluster) concentration can be expressed in the form

$$x_v = x_{v0}\exp\left(-e_f^{\mathrm{cl}}/kT\right). \tag{22}$$

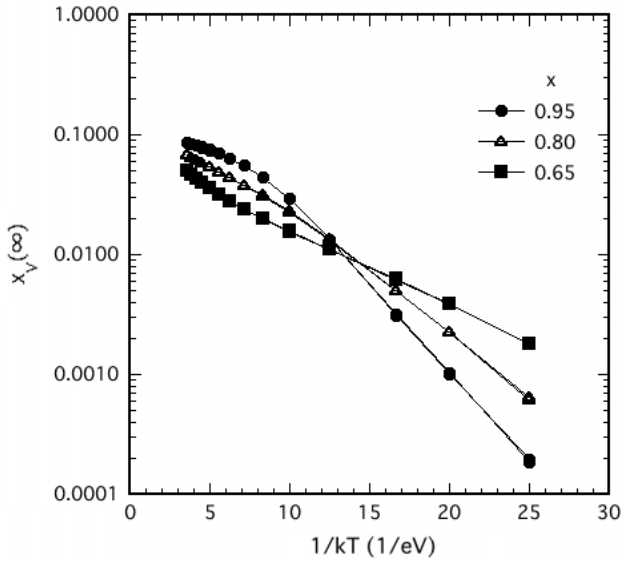

Figure 20. Arrhenius plot of the vacancy concentration in the closed system, calculated for the H concentrations $x = 0.65$, 0.80 and 0.95, with $e_b = 0.34$ eV. The system stays in the 'vacancy-poor' state over the whole temperature range. The vacancy (Vac–H cluster) formation is described by a simple thermal activation process at low vacancy concentrations ($x_v \leqslant 0.03$).

Table 1. Vacancy concentration in the 'vacancy-poor' phase ($e_b = 0.34$ eV) at low vacancy concentrations ($x_v \leqslant 0.03$).

	From Arrhenius plot		From equations (23)–(25)	
x	x_{v0}	e_f^{cl} (eV)	x_{v0}	e_f^{cl} (eV)
0.65	0.07	0.14	0.075	0.15
0.80	0.26	0.24	0.26	0.24
0.95	0.89	0.34	0.74	0.33

The pre-exponential factor and the activation energy derived from the Arrhenius fit are given in table 1. Anticipating the relations

$$x_{v0} \approx x^6, \tag{23}$$

$$e_f^{cl} = u_v - 6e_b + \alpha_v \Delta \tag{24}$$

to hold, and approximating the dilatation to be primarily determined by H atoms, i.e.

$$\alpha_v \Delta \approx (3\alpha_H^2/\gamma B\Omega_0)x, \tag{25}$$

we may estimate x_{v0} and e_f^{cl} as listed in table 1. These estimates agree excellently with those derived from the Arrhenius plot. Note that the large dependence of the cluster formation energy on H concentration comes through the long-range elastic interaction. Note, also, that the relation $x_{v0} \approx x^6$ is a consequence of having neglected the changes in the vibrational states in the reaction $\mathrm{Vac} + 6\mathrm{H} \rightarrow \mathrm{VacH_6}$. More generally, there must be a multiplicative factor $\exp(\Delta s_f^{cl}/k)$ arising from the change in the vibrational entropy in the cluster formation. Crude estimates from experiments on γ-Fe [7] and Pd [9] suggest the multiplicative factor of $\sim 10^3$ ($\Delta s_f^{cl}/k = 7$–8). This is consistent, at least qualitatively, with the lowering of the vibrational frequencies expected for H atoms trapped by vacancies.

Experimental results obtained by the closed-system method (figure 2) may be compared with theoretical results for $T = 1160$ K (figure 8(a)). The results for NbH_x ($x \leqslant 0.5$) appear to correspond to the case of low e_bs, whereas those for PdH_x($x < 0.8$) are more likely to correspond to the case of intermediate e_bs. (The data for high H concentrations in PdH_x, taken by the open-system method, will be examined in the next section.)

4.3. Analysis of the results for the open system

Comparison of the calculated results for the closed-system method (figure 8(a)) and the open-system method (figure 9) for the same temperature, may appear to indicate that overall features are very similar. Indeed, for small e_bs ($e_b < 0.36$ eV), the $\Omega(0) - \Omega(\infty)$ versus $x(0)$ relations are nearly identical. For larger $e_b s$ ($e_b > 0.41$ eV), however, a small difference in the $\Omega(0) - \Omega(\infty)$ versus $x(0)$ relation originates, in fact, from very different underlying mechanisms, as manifested in the variation of H and vacancy concentrations. Figures 10 and 11 show that, for $e_b < 0.36$ eV, both H and vacancy concentrations remain close to their original values ($x(\infty) \approx x(0)$, $x_v(\infty) \approx 0$), whereas for $e_b > 0.41$ eV, they increase abruptly at rather small H concentrations to their ultimate values ($x(\infty) \approx 0.8$, $x_v(\infty) \approx 0.25$). This implies that, for large $e_b s$, H and vacancies are introduced as Vac–H clusters, so that the ultimate composition $M_3VacH_{\sim 3}$ may be reached, even for small initial H concentrations.

Inspection of data obtained for Fe–H, Co–H and Ni–H systems (figures 5–7) shows that, in these cases, the ultimate defect hydrides are formed immediately, suggesting that they correspond to the case of large e_bs. For PdH_x ($x \sim 1$), the final volume contraction amounts to 1/3–1/2 of the other cases, which suggests that the system corresponds to the case of intermediate e_b. This is consistent with the conclusion reached from the closed-system experiments.

4.4. Additional remarks

Here we make some remarks regarding the implication of the present result for defect-hydride formation in general. Although the calculation was performed for the specific case of fcc defect hydrides, taking the Ni–H system as an example, the essence of the results, i.e. the occurrence of two-phase separation into 'vacancy-poor' and 'vacancy-rich' states, is believed to be quite general.

In actual situations, the occurrence of two-phase separation depends on several factors:

First, the binding energy should be large enough to make the formation energy of a Vac–H cluster small enough.

Second, the chemical potential of H should be high enough to sustain high interstitial H concentrations, and large occupation numbers of trapped H atoms as well.

Third, the temperature should be lower than the critical temperature of the two-phase separation, but high enough to allow phase separation to take place within reasonable lengths of time. Judging from the simulation results on Ni, the critical temperature under the combined action of local configurational effects and long-range elastic interactions appears to be high enough to sustain phase separation even up to the melting point of metals.

Fourth, the type of crystal structure is most favorable for fcc, less for bcc and least for hcp. This is because the formation of the ultimate defect-ordered structure appears more easily attainable in fcc hydrides than in bcc-based hydrides. In the hcp phase, as binding energies are generally small [14, 16, 21], formation of the 'vacancy-rich state' appears unlikely.

The reason why defect hydrides of high vacancy concentrations were frequently observed in fcc metal hydrides is because these conditions are more easily satisfied in fcc hydrides under actual experimental conditions than in other cases.

In closing this section, a few words of caution may be in order as regards the 'vacancy-poor' state, in order to avoid possible confusion. The point is that even the 'vacancy-poor' state has concentrations of Vac–H clusters many orders of magnitude higher in comparison to vacancy concentrations in pure metals, and certainly deserves the name of superabundant vacancies. For example, in the case of Nb at 300 °C, a vacancy concentration in pure Nb is estimated at 10^{-25}, whereas the concentration of Vac–H clusters in $NbH_{0.23}$ is 10^{-3} [18]; 22 orders of magnitude larger! Under ordinary conditions, the 'vacancy-rich' states are not easily realized, but the 'vacancy-poor' states are. Our experience shows that after hydrogenation of metal specimens, either by high p_H, T treatment or by electrolytic deposition, Vac–H clusters of concentrations 10^{-4}–10^{-3} were retained and remained stable under ambient conditions for indefinite lengths of time ($\geqslant$10 years). These concentrations are high enough to exert significant influence on materials properties, e.g. the diffusion of M-atoms and the stability of electro-deposited metals and alloys. These H-induced effects have been attracting increasing interest in the last years [53–55].

Further characterization of SAV formation in the 'vacancy-poor' state by experiments, a problem of more importance for practical purposes, is left for future studies.

5. Summary

The formation of defect structure with superabundant M-atom vacancies has been studied on fcc-based M–H alloys. Two distinctly different states, the 'vacancy-poor' state and the 'vacancy-rich' state, have been observed, and explained, both experimentally and theoretically, in terms of phase separation under the combined action of long-range elastic interactions and local configurational effect arising from Vac–H interactions.

Acknowledgments

This report is based on SAV formation experiments performed by many collaborators. We wish to thank all the members of Fukai's laboratory for their enormous effort expended in the last 15 years, and especially to S Harada for his heuristic analysis of all the existing data (figures 5–7). The XRD measurements under high pH, T conditions were made at a synchrotron facility in Tsukuba (Photon Factory, Institute of Materials Structure Science, KEK), under Approval 92-128, 93G151, 94G151, 96G118, 98G049, 00G027 and 02G028. We gratefully acknowledge the continuing support of T Kikegawa of KEK for the whole period of time. We also thank D Ono for his assistance in the initial stage of Monte Carlo simulations.

References

[1] Fukai Y and Ōkuma N 1993 *Japan. J. Appl. Phys.* **32** L1256
[2] Fukai Y and Ōkuma N 1994 *Phys. Rev. Lett.* **73** 1640
[3] Ōsono H, Kino T, Kurokawa Y and Fukai Y 1995 *J. Alloys Compounds* **231** 41
[4] Nakamura K and Fukai Y 1995 *J. Alloys Compounds* **231** 46
[5] Fukai Y, Kurokawa Y and Hiraoka H 1997 *J. Japan Inst. Met.* **61** 663
[6] Birnbaum H K, Buckley C, Zaides F, Sirois E, Rosenak P, Spooner S and Lin J S 1997 *J. Alloys Compounds* **253/254** 260
[7] Iwamoto M and Fukai Y 1999 *Trans. Japan Inst. Met.* **40** 606
[8] dos Santos D S, Miraglia S and Fruchart D 1999 *J. Alloys Compounds* **291** L1
[9] Fukai Y, Ishii Y, Goto T and Watanabe K 2000 *J. Alloys Compounds* **313** 121
[10] Miraglia S, Fruchart D, Hlil E K, Tavares S S M and dos Santos D 2001 *J. Alloys Compounds* **317** 77

[11] Fukai Y, Haraguchi T, Hayashi E, Ishii Y, Kurokawa Y and Yanagawa J 2001 *Defect Diffusion Forum* **194–199** 1063
[12] Fukai Y, Shizuku Y and Kurokawa Y 2001 *J. Alloys Compounds* **329** 195
[13] Buckley C E and Birnbaum H K 2002 *J. Alloys Compounds* **330–332** 649
[14] Fukai Y and Mizutani M 2002 *Mater. Trans.* **43** 1079
[15] Fukai Y, Mori K and Shinomiya H 2003 *J. Alloys Compounds* **348** 105
[16] Fukai Y and Mizutani M 2003 *Mater. Trans.* **44** 1359
[17] Fukai Y, Mizutani M, Yokota S, Kanazawa M, Miura Y and Watanabe T 2003 *J. Alloys Compounds* **356/357** 270
[18] Koike H, Shizuku Y, Yazaki A and Fukai Y 2004 *J. Phys.: Condens. Matter* **16** 1335
[19] Hiroi T, Fukai Y and Mori K 2005 *J. Alloys Compounds* **404–406** 252
[20] Harada S, Yokota S, Ishii Y, Shizuku Y, Kanazawa M and Fukai Y 2005 *J. Alloys Compounds* **404–406** 247
[21] Fukai Y, Yokota S and Yanagawa J 2006 *J. Alloys Compounds* **407** 16
[22] Fukai Y 1995 *J. Alloys Compounds* **231** 35
[23] Fukai Y 2003 *J. Alloys Compounds* **356/357** 263
[24] Fukai Y 2003 *Phys. Scr.* **T 103** 11
[25] Fukai Y 2005 *The Metal-Hydrogen System* 2nd edn (Berlin: Springer) section 5.6
[26] Watanabe K, Ōkuma N, Fukai Y, Sakamoto Y and Hayashi Y 1996 *Scr. Mater.* **34** 551
[27] Hayashi E, Kurokawa Y and Fukai Y 1998 *Phys. Rev. Lett.* **80** 5588
[28] Yamazaki Y and Iijima Y 2004 *Defect Diffus. Forum* **233/234** 115
[29] Yamazaki Y, Iijima Y and Okada M 2004 *Acta Mater.* **52** 1247
[30] Yamazaki Y, Iijima Y and Okada M 2004 *Phil. Mag. Lett.* **84** 165
[31] Iida T, Yamazaki Y, Kobayashi T, Iijima Y and Fukai Y 2005 *Acta Mater.* **53** 3083
[32] Möller W, Besenbacher F and Bøttiger J 1982 *Appl. Phys.* A **27** 19
[33] Myers S M, Richards P M, Wampler W R and Besenbacher F 1989 *J. Nucl. Mater.* **165** 9
[34] Myers S M, Nordlander P, Besenbacher F and Nørskov J K 1986 *Phys. Rev.* B **33** 851
[35] Tateyama Y and Ohno T 2003 *Phys. Rev.* B **67** 174105
[36] Lu G and Kaxiras E 2005 *Phys. Rev. Lett.* **94** 155501
[37] Hlil E K, Fruchart D, Miraglia S and Tabola J 2003 *J. Alloys Compounds* **356/357** 169
[38] dos Santos D, Tavares S S M, Miraglia S, Fruchart D and dos Santos D R 2003 *J. Alloys Compounds* **356/357** 258
[39] Zhang C and Alavi A 2005 *J. Am. Chem. Soc.* **127** 9808
[40] Semilenov S A, Baranova R V, Khodyrev Yu P and Imanov R M 1980 *Sov. Phys. Crystallogr.* **25** 665
[41] Fukai Y, Yamakata M and Yagi T 1993 *Z. Phys. Chem.* **179** 119
[42] Harada S, Ono D, Sugimoto H and Fukai Y 2007 *J. Alloys Compounds* at press
[43] Antonov V E, Belash I T, Pomomarev B K, Ponyatovsky E G and Thiessen V G 1979 *Phys. Status Solidi* a **52** 703
[44] Korzhavyi P A, Abrikosov I A, Johansson B, Ruban A V and Skriver H L 1999 *Phys. Rev.* B **59** 11693
[45] Eshelby J D 1956 *Solid State Physics* vol 2, ed F Seitz and D Turnbull (New York: Academic) p 79
[46] Fukai Y 2005 *The Metal-Hydrogen System* 2nd edn (Berlin: Springer) section 2.2
[47] Wagner H 1978 *Hydrogen in Metals I* ed G Alefeld and J Völkl (Berlin: Springer) p 5
[48] Fukai Y 2005 *The Metal-Hydrogen System* 2nd edn (Berlin: Springer) section 2.3
[49] Ehrhart P, Jung P, Schultz H and Ullmaier H 1993 *Atomic Defects in Metals* (*Landolt-Börnstein New Series* vol 25) ed H Ullmaier (Berlin: Springer)
[50] Fukai Y 2005 *The Metal-Hydrogen System* 2nd edn (Berlin: Springer) section 4.2
[51] Fukai Y, Yamamoto S, Harada S and Kanazawa M 2004 *J. Alloys Compounds* **372** L4
[52] Fukai Y 2005 *J. Alloys Compounds* **404–406** 7
[53] Fujikawa T, Yoshikawa T, Ohnishi T and Sato T 2001 *Japan. J. Appl. Phys.* **40** 2191
[54] Fukai Y, Hiroi T, Mukaibo N and Shimizu Y 2007 *J. Japan Inst. Met.* **71** 388
[55] Mukaibo N, Shimizu Y, Fukai Y and Hiroi T 2007 *J. Japan Inst. Met.* **71** 809